Energy-Loss Spectrum of Fast Electrons in a Dielectric Slab. I. Nonretarded Losses and Cherenkov Bulk Loss

A. A. LUCAS* AND E. KARTHEUSER
Department of Theoretical Physics, University of Liège, Liège, Belgium
(Received 3 November 1969)

The energy lost, in the phonon-energy range, by a fast electron beam passing through a polar dielectric slab is analyzed using classical electrodynamics. The medium is represented by a frequency-dependent dielectric constant $\epsilon(\omega)=\epsilon_\infty(\omega_L^2-\omega^2)/(\omega_T^2-\omega^2)$ having one single pole at the transverse optical-phonon frequency ω_T and one zero at the longitudinal-mode frequency ω_L. When retardation effects are excluded ($c=\infty$), two kinds of losses occur: bulk losses resulting from the emission of the longitudinal optical phonon at ω_L and surface losses due to the excitation of "surface" vibrations whose frequencies lie within the gap (ω_T,ω_L). Both effects can be obtained exactly in terms of closed analytic functions of ω. When retardation is taken into account, radiation losses take place as well, either through Cherenkov radiation in the bulk of the slab or through the so-called "transition radiation" occuring at the surfaces of the slab. Here we will study the Cherenkov loss only. Surface radiative losses are treated in part II. Comparison with experimental results for alkali-halide crystals and with calculations due to Fujiwara and Ohtaka is presented.

INTRODUCTION

THE accuracy with which the energy distribution of a fast electron beam can be measured has reached such a point that it is now possible to detect energy losses suffered by the beam in the optical-phonon energy range of the irradiated crystal. Thus Boersch *et al.*[1] obtained high-resolution energy-loss spectra for 25-keV electrons passing through thin LiF crystal slabs in the region of the TO-LO energy range of this material (see Fig. 1). They suggested that the observed spectrum and particularly its dependence on the slab thickness could be due to the excitation of surface optical phonons rather than to the interaction with the bulk longitudinal optical phonon which should normally dominate for thick crystals.

Recently, Fujiwara, and Ohtaka[2] attempted to verify this interpretation by computing numerically a theoretical loss function previously derived by Ritchie.[3] In this theory, the *quasistatic* (nonretarded) Maxwell equations are used to describe the interaction between the electron and the dielectric slab. The latter is simply represented by a continuous medium with the frequency-dependent (quasistatic) dielectric function

$$\epsilon(\omega)=\epsilon_\infty+\frac{\epsilon_0-\epsilon_\infty}{1-\omega^2/\omega_T^2-i\gamma(\omega/\omega_T)}, \qquad (1)$$

where ϵ_0 and ϵ_∞ are the static and high-frequency dielectric constants, respectively, and where ω_T and $\omega_L=\omega_T(\epsilon_0/\epsilon_\infty)^{1/2}$ are the usual TO and LO phonon-mode frequencies; γ is a small damping constant.

Two kinds of losses are obtained: on the one hand, a narrow band centered at ω_L and proportional to the bulk loss function $\mathrm{Im}(1/\epsilon)$; on the other hand, a broad asymmetrical band extending between ω_T and ω_L and resulting from the coupling of the electron to the surface vibrational modes of the slab. For slab thicknesses smaller than $\sim$1000 Å, surface-mode excitations indeed seem to provide the dominant loss mechanism as suggested by the measurements on LiF.[1]

The present work has two purposes. First, we want to reconsider the nonretarded loss function as obtained by Ritchie[3] and show that it can be integrated analytically to provide the exact loss spectrum, at least in the case where $\epsilon(\omega)$ is real. An imaginary part in ϵ, small as it is for ionic crystals ($\gamma\simeq0.04$), can only give a slight correction to this exact result. We found that the general shape of the spectrum agrees with the one numerically obtained by Fujiwara and Ohtaka,[2] although the amplitude of the surface losses relative to the bulk ones seems to have been overestimated by about a factor 2 in their calculations.

The second and main purpose of our work is to analyze the problem from the full set of Maxwell equations, radiative effects included. Emission of radiation by energetic charged particles passing through matter has been extensively investigated, in particular by Ritchie and others[4,5] and by numerous workers in the Russian literature.[6] Most of these works are concerned with the photon distribution in the frequency region corresponding to plasma excitation. Here we want to apply the theory to the phonon-energy region, concentrating primarily on the loss function rather than on the photon production. Two new kinds of losses occur which are not present in the quasistatic case. First some energy is converted into ordinary Cherenkov radiation in that frequency range for which $v^2>c^2/\epsilon(\omega)$, where v is the velocity of the electron. This bulk effect is shown to contribute a low-energy tail ($\hbar\omega<\hbar\omega_T$) to the nonretarded loss spectrum. We also establish the

* Chargé de Recherches au Fonds National Belge de la Recherche Scientifique.

[1] H. Boersch, J. Geiger, and W. Stickel, Phys. Rev. Letters **17**, 379 (1966).

[2] T. Fujiwara and K. Ohtaka, J. Phys. Soc. Japan **24**, 1326 (1968).

[3] R. H. Ritchie, Phys. Rev. **106**, 874 (1957).

[4] R. H. Ritchie and H. B. Eldridge, Phys. Rev. **126**, 1935 (1961).

[5] J. C. Ashley and R. H. Ritchie, J. Appl. Phys. **35**, 2313 (1964).

[6] V. E. Pafomov, Zh. Eksperim. i Teor. Fiz. **39**, 134 (1960) [Soviet Phys. JETP **12**, 97 (1961)].

connection between this result and the theory of the Cherenkov effect such as presented in a classical paper by Fermi.[7] Second, photons are also generated by the excitation of the so-called "radiative polariton modes." Here we use the nomenclature introduced by Kliewer and Fuchs in their interpretation of far-infrared absorption of ionic crystals.[8] Alternatively, one can describe this mechanism as energy lost through "transition radiation."[9] This is a surface loss which will be studied in a subsequent publication.

The paper is divided into four sections. In Sec. 1 the general solutions of Maxwell's equations are obtained and the loss function is defined. Section 2 is devoted to the derivation of the loss spectrum in the quasistatic approximation. In Sec. 3 we study the Cherenkov-loss mechanism. Comparison with previous experimental and theoretical works is given in Sec. 4.

1. MAXWELL EQUATIONS AND LOSS FUNCTION

In this section, we write the general solutions of the Maxwell equations for the dielectric slab in the presence of a uniformly moving charge density $-e\delta(\boldsymbol{\varrho})\delta(z-vt)$, where $\boldsymbol{\varrho}=(x,y)$ (Fig. 2). The electromagnetic fields are Fourier analyzed with respect to time t and $\boldsymbol{\varrho}$:

$$\mathbf{E}(\boldsymbol{\varrho},z,t)=(2\pi)^{-3}\int d\mathbf{k}_\perp\int d\omega\,\mathbf{E}(\mathbf{k}_\perp,\omega,z)\times\exp i(\mathbf{k}_\perp\cdot\boldsymbol{\varrho}-\omega t),\quad\text{etc.}\quad(2)$$

Eliminating the magnetic fields from the Maxwell equations in the usual way, one finds the following propagation equations for the component $E_\perp=\mathbf{E}(\mathbf{k}_\perp,\omega,z)\cdot\mathbf{k}_\perp/k_\perp$:

$$\frac{d^2E_\perp}{dz^2}-\alpha^2E_\perp=-ik_\perp\frac{4\pi e}{v\epsilon}e^{i(\omega/v)z},\quad(3)$$

where

$$\alpha^2=k_\perp{}^2-\epsilon(\omega)(\omega^2/c^2).\quad(4)$$

The component E_z is related to $E_\perp$ by

$$E_z=-ik_\perp\int E_\perp dz+i\frac{4\pi e}{\omega\epsilon}e^{i(\omega/v)z}.\quad(5)$$

The general solution of (3) is

$$E_\perp=ae^{\alpha z}+be^{-\alpha z}+ik_\perp(4\pi e/\epsilon v\xi^2)e^{i(\omega/v)z},\quad(6)$$

and from (5)

$$E_z=-i(k_\perp/\alpha)(ae^{\alpha z}-be^{-\alpha z})+i(4\pi e\omega/\epsilon v^2\xi^2)\beta^2e^{i(\omega/v)z},\quad(7)$$

where

$$\xi^2=k_\perp{}^2+(\omega^2/v^2)\beta^2,\quad\beta^2=1-\epsilon(\omega)(v^2/c^2),\quad(8)$$

[7] E. Fermi, Phys. Rev. **57**, 485 (1940).
[8] K. L. Kliewer and R. Fuchs, Phys. Rev. **150**, 573 (1966).
[9] I. M. Frank and V. I. Ginsburg, J. Phys. (USSR) **9**, 353 (1945).

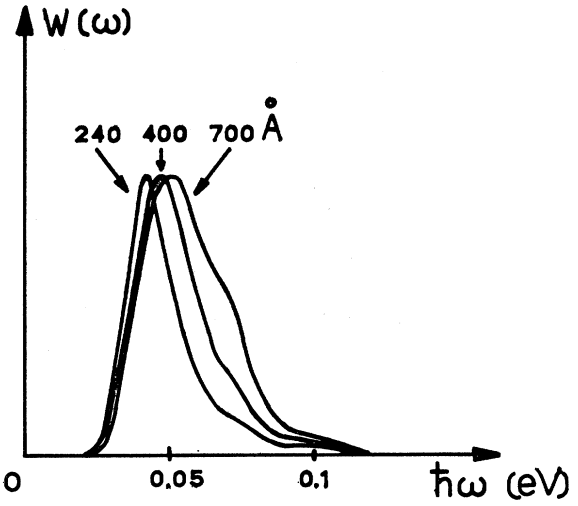

FIG. 1. Energy-loss spectra of 25-keV electrons in LiF slab deposited on carbon substrate, for three different thicknesses (Ref. 1).

and where a, b are arbitrary integration constants. These constants are determined by the boundary conditions imposed at $z=\pm\infty$ and by the continuity conditions of the fields at $z=\pm z_0$ (Fig. 2). Here two cases have to be distinguished according to whether the quantity $\alpha_0{}^2=k_\perp{}^2-\omega^2/c^2$ is positive or negative. In the first case where α_0 is real positive, we must choose exponentially decreasing fields outside the slab and we are then describing the coupling of the electron to the real, localized phonon modes of the dielectric slab, as depicted in Fig. 3(a). In the second case for which $\alpha_0{}^2<0$ or $\alpha_0=i\delta_0$ with δ_0 real positive, we are dealing with the interaction of the beam with the so-called

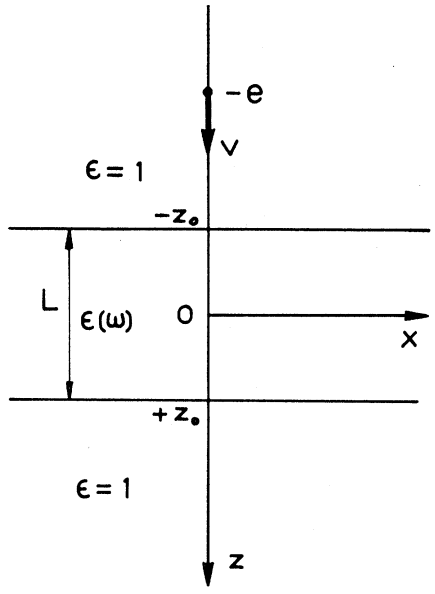

FIG. 2. Geometry of the energy-loss experiment. The electron is moving along the z axis, in the $+z$ direction.

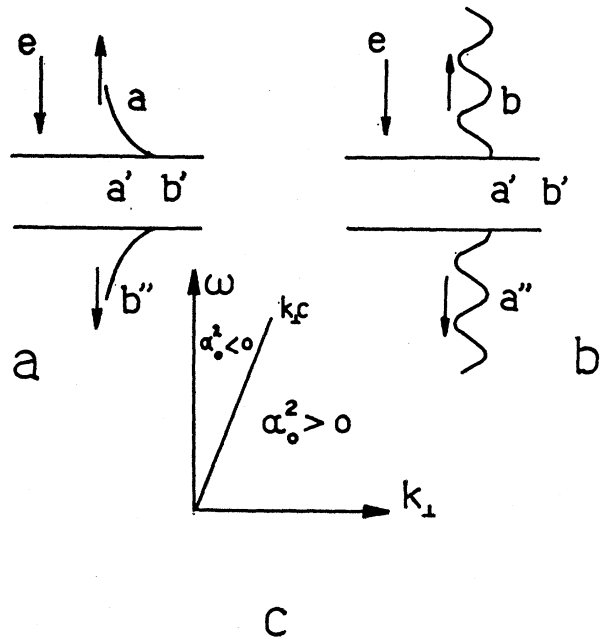

FIG. 3. (a) Boundary conditions to be imposed on the fields. For the region $\alpha_0>0$ of the $(\omega,k\epsilon)$ plane shown in (c) the primary electron field $\exp[i(\omega/v)z]$ has to match exponentially decreasing fields outside the slab. (b) For $\alpha_0=i\delta_0$, $\delta_0>0$, we have radiation flowing out of the slab excited by the electron field.

"virtual" or "radiative modes"[8] which induce oscillatory fields outside the slab. This case is sketched in Fig. 3(b). Referring to the notations of Fig. 3(a), where $\alpha_0>0$, the continuity conditions of $E_\perp(z)$ and $\epsilon E_z(z)$ at $z=\pm z_0$, write

$$\begin{bmatrix} e^{-\alpha_0 z_0} & -e^{-\alpha z_0} & -e^{\alpha z_0} & 0 \\ 0 & -e^{\alpha z_0} & -e^{-\alpha z_0} & e^{-\alpha_0 z_0} \\ -\frac{ik_\perp}{\alpha_0}e^{-\alpha_0 z_0} & \frac{ik_\perp\epsilon}{\alpha}e^{-\alpha z_0} & -\frac{ik_\perp\epsilon}{\alpha}e^{\alpha z_0} & 0 \\ 0 & \frac{ik_\perp\epsilon}{\alpha}e^{\alpha z_0} & -\frac{ik_\perp\epsilon}{\alpha}e^{-\alpha z_0} & \frac{ik_\perp}{\alpha_0}e^{-\alpha_0 z_0} \end{bmatrix} \begin{bmatrix} a \\ a' \\ b' \\ b'' \end{bmatrix} = i\frac{4\pi e}{v} \begin{bmatrix} \eta e^{-i(\omega/v)z_0} \\ \eta e^{i(\omega/v)z_0} \\ \gamma e^{-i(\omega/v)z_0} \\ \gamma e^{i(\omega/v)z_0} \end{bmatrix}, \quad (9)$$

where

$$\eta=k_\perp(1/\epsilon\xi^2-1/\xi_0^2), \qquad \gamma=(\omega/v)(\beta^2/\xi^2-\beta_0^2/\xi_0^2), \quad (10)$$

the index 0 meaning that ϵ has to be replaced by 1 in the corresponding quantity. The solutions of (9) are

$$a=\Delta_a/\Delta, \quad a'=\Delta_{a'}/\Delta, \quad b'=\Delta_{b'}/\Delta, \quad b''=\Delta_{b''}/\Delta, \quad (11)$$

where

$$\Delta=-k_\perp^2 e^{-\alpha_0 L}\left[e^{\alpha L}\left(\frac{\epsilon}{\alpha}+\frac{1}{\alpha_0}\right)^2-e^{-\alpha L}\left(\frac{\epsilon}{\alpha}-\frac{1}{\alpha_0}\right)^2\right], \quad (12)$$

$$\begin{aligned}\Delta_a=\frac{4\pi e}{v}k_\perp\Bigg\{&\left(\frac{\epsilon}{\alpha}-\frac{1}{\alpha_0}\right)\left(\gamma+i\eta\frac{k_\perp\epsilon}{\alpha}\right)\\ &\times\exp\left[-\left(2\alpha+\alpha_0+i\frac{\omega}{v}\right)\frac{L}{2}\right]\\ &+\left(\frac{1}{\alpha_0}+\frac{\epsilon}{\alpha}\right)\left(\gamma-i\eta\frac{k_\perp\epsilon}{\alpha}\right)\exp\left[\left(2\alpha-\alpha_0-i\frac{\omega}{v}\right)\frac{L}{2}\right]\\ &-2\frac{\epsilon}{\alpha}\left(\gamma-i\eta\frac{k_\perp}{\alpha_0}\right)\exp\left[-\left(\alpha_0-i\frac{\omega}{v}\right)\frac{L}{2}\right]\Bigg\}, \end{aligned} \quad (13)$$

$$\begin{aligned}\Delta_{a'}=-\frac{4\pi e}{v}k_\perp e^{-\alpha_0 L}\Bigg\{&-\left(\frac{\epsilon}{\alpha}-\frac{1}{\alpha_0}\right)\left(\gamma+i\frac{k_\perp\eta}{\alpha_0}\right)\\ &\times\exp\left[-\left(\alpha+i\frac{\omega}{v}\right)\frac{L}{2}\right]+\left(\frac{1}{\alpha_0}+\frac{\epsilon}{\alpha}\right)\left(\gamma-i\frac{k_\perp\eta}{\alpha_0}\right)\\ &\times\exp\left[\left(\alpha+i\frac{\omega}{v}\right)\frac{L}{2}\right]\Bigg\}, \end{aligned} \quad (14)$$

$$\Delta_{b''}(v)=-\Delta_a(-v), \quad \Delta_{b'}(v)=-\Delta_{a'}(-v). \quad (15)$$

The case sketched in Fig. 3(b) is similar. The coefficients Δ, Δ_b, $\Delta_{a'}$, $\Delta_{b'}$, $\Delta_{a''}$ appropriate to this case can be obtained from the previous ones simply by substituting $-i\delta_0$ for α_0 in (12) to (15), respectively.

Once the fields are specified, one can obtain the energy loss suffered by the particle in two ways. Following Fermi's method[7] one can compute the flux of the Poynting vector through a cylinder surface of radius R centered on the path of the particle, thus obtaining the energy lost outside the cylinder. When R is of the order of atomic distances, what is lost inside the cylinder cannot be computed with classical electrodynamics of continuous media. Another definition, completely equivalent as we shall see, is to identify the energy loss to the work done by the fields on the particle:

$$\begin{aligned}W_{\text{total}}&=\int_{-\infty}^{+\infty}dz\,e\left(\mathbf{E}+\frac{1}{c}\mathbf{v}\times\mathbf{H}\right)_{z,\rho=0,t=z/v}\\ &=\int_{-\infty}^{+\infty}dz\,eE_z(\boldsymbol{\rho}=0,t=z/v), \end{aligned} \quad (16)$$

where the z component of the field has to be taken at the actual position of the electron. There is no need to substract the vacuum field of the electron from this definition as this field does not do any work. Introduc-

ing the real part of (2) into (16), one gets

$$W_{\text{total}}=(2\pi)^{-3}$$

$$\times\mathrm{Re}\left[\int d\mathbf{k}_\perp\int d\omega\int_{-\infty}^{+\infty}dz\, eE_z(k_\perp,\omega,z)e^{-i(\omega/v)z}\right] \quad (17)$$

or

$$W_{\text{total}}=\int_0^\infty 2\pi k_\perp dk_\perp\int_{-\infty}^{+\infty}d\omega\,\hbar\omega P(k_\perp,\omega)\,, \quad (18)$$

where one has defined the classical probability $P(k_\perp,\omega)$ for the electron to lose the energy $\hbar\omega$:

$$P(k_\perp,\omega)=(2\pi)^{-3}\,\mathrm{Re}\left[\int_{-\infty}^{+\infty}dz\frac{e}{\hbar\omega}E_z(k_\perp,\omega,z)e^{-i(\omega/v)z}\right]. \quad (19)$$

This classical limit of the true quantum loss function is meaningful only insofar as one can treat the medium as continuous, i.e., when the wave vector $k_\perp$ is much smaller than the inverse of atomic distances. Accordingly the contribution to the $k_\perp$ integral (18) coming from values of $k_\perp$ larger than this classical limit $K_c\sim1$ Å^{-1} must be disregarded. Actually the part of the integral

$$\int_{K_c}^\infty k_\perp dk_\perp P(k_\perp,\omega)$$

provides the energy which the electron loses within a region of radius K_c^{-1} around its trajectory as can be seen by changing the integration variable from $k_\perp$ to $\rho=k_\perp^{-1}$. As emphasized by Fermi,[7] this contribution cannot be treated classically.

In the experiments of Boersch *et al.*,[1] on the other hand, one does not collect electrons which have been scattered to an angle larger than a certain small value $\theta_0\sim10^{-4}$ rad off the axis of the primary beam. This provides an experimental limit to the momentum transfer determined by the energy and momentum conservation equation $\hbar^2K^2/2m=E_0\theta_0^2$, where E_0 is the energy of the incident beam. For $E_0\sim25$ keV, one finds that $K\ll K_c$ and, therefore,

$$W=2\pi\int_0^K k_\perp dk_\perp\int_{-\infty}^{+\infty}\hbar\omega P(k_\perp,\omega)d\omega \quad (20)$$

should provide a good representation of the observed total loss.

Substituting (7) into (19) we find for the loss function $P(k_\perp,\omega)$, taking (15) into account (and writing k for $k_\perp$),

$$P(k,\omega)=P_S(k,\omega)+P_B(k,\omega)\,, \quad (21)$$

where

$$P_S(k,\omega)=-(2\pi)^{-3}\,\mathrm{Im}\left[\frac{ek}{\hbar\omega}\frac{1}{\Delta}\left(\frac{e^{-(\alpha_0-i(\omega/v))z_0}}{\alpha_0(\alpha_0-i(\omega/v))}\Delta_a\right.\right.$$

$$\left.\left.+2\frac{\sinh(\alpha-i(\omega/v))z_0}{\alpha(\alpha-i(\omega/v))}\Delta_{a'}+(\text{same with } v\to-v)\right)\right] \quad (22)$$

and

$$P_B(k,\omega)=-\frac{e^2L}{2\pi^2\hbar v^2}\,\mathrm{Im}\frac{\beta^2}{\epsilon\xi^2}\,. \quad (23)$$

These are the surface and bulk loss probabilities, respectively. Using (13) and (14), $P_s(k,\omega)$ is given explicitly by

$$P_S(k,\omega)=\frac{-e^2}{\pi^2\hbar\omega v}\,\mathrm{Im}\frac{1}{\Delta'}\left\{-\frac{2}{\alpha}\left[\epsilon\gamma\left(\frac{1}{\xi^2}-\frac{1}{\xi_0^2}\right)+\epsilon\frac{\eta^2}{\alpha_0^2}\frac{\omega}{v}\right]\right.$$

$$\times\cos\frac{\omega L}{v}+4\frac{\epsilon\gamma\eta}{\alpha_0\alpha}\frac{\omega}{v}\sin\frac{\omega L}{v}+\gamma\left(\frac{1}{\xi^2}-\frac{1}{\xi_0^2}\right)$$

$$\times\left[\left(\frac{1}{\alpha_0}+\frac{\epsilon}{\alpha}\right)e^{\alpha L}-\left(\frac{1}{\alpha_0}-\frac{\epsilon}{\alpha}\right)e^{-\alpha L}\right]$$

$$\left.+\frac{\epsilon\eta^2}{\alpha_0\alpha}\frac{\omega}{v}\left[\left(\frac{1}{\alpha_0}+\frac{\epsilon}{\alpha}\right)e^{\alpha L}+\left(\frac{1}{\alpha_0}-\frac{\epsilon}{\alpha}\right)e^{-\alpha L}\right]\right\}\,, \quad (24)$$

where

$$\Delta'=(1/\alpha_0-1/\alpha)^2e^{-\alpha L}-(1/\alpha_0+1/\alpha)e^{\alpha L}. \quad (25)$$

This is the correct surface loss function for the case where α_0 is real positive. One obtains the loss due to the excitation of virtual or radiative modes by substituting $-i\delta_0\equiv-i(\omega^2/c^2-k^2)^{1/2}$ for α_0 in (24).

2. QUASISTATIC LOSS SPECTRUM

Taking the limit $c\to\infty$, one has $\alpha=\alpha_0=k$, $\xi^2=k^2+\omega^2/v^2$ and, after some simplification, the previous results reduce to

$$P_S^{\mathrm{NR}}=-\frac{e^2}{2\pi^2\hbar v^2}\frac{2k}{(k^2+\omega^2/v^2)^2}\,\mathrm{Im}\left[\frac{1-\epsilon}{\epsilon}\right.$$

$$\left.\times\frac{2(\epsilon-1)\cos(\omega L/v)+(1-\epsilon^2)e^{kL}+(1-\epsilon)^2e^{-kL}}{(1-\epsilon)^2e^{-kL}-(1+\epsilon)^2e^{kL}}\right]. \quad (26a)$$

$$P_B^{\mathrm{NR}}=-\frac{e^2L}{2\pi^2\hbar v^2}\frac{1}{k^2+\omega^2/v^2}\,\mathrm{Im}\frac{1}{\epsilon}\,. \quad (26b)$$

This is the loss function obtained for the first time by Ritchie[3] in his treatment of losses due to the excitation of electronic plasmons in metallic foils. The only difference with the present case is in the form of the dielectric constant and in the energy range of interest. The same result has been rederived later, in particular by Hattori and Yamada[10] and, more recently, by Fujiwara and Ohtaka.[2]

Now one can define the nonretarded loss spectrum

$$W^{\mathrm{NR}}(\omega)=2\pi\int_0^K kdk\,P^{\mathrm{NR}}(k,\omega). \quad (27)$$

[10] M. Hattori and K. Yamada, J. Phys. Soc. Japan **18**, 200 (1963).

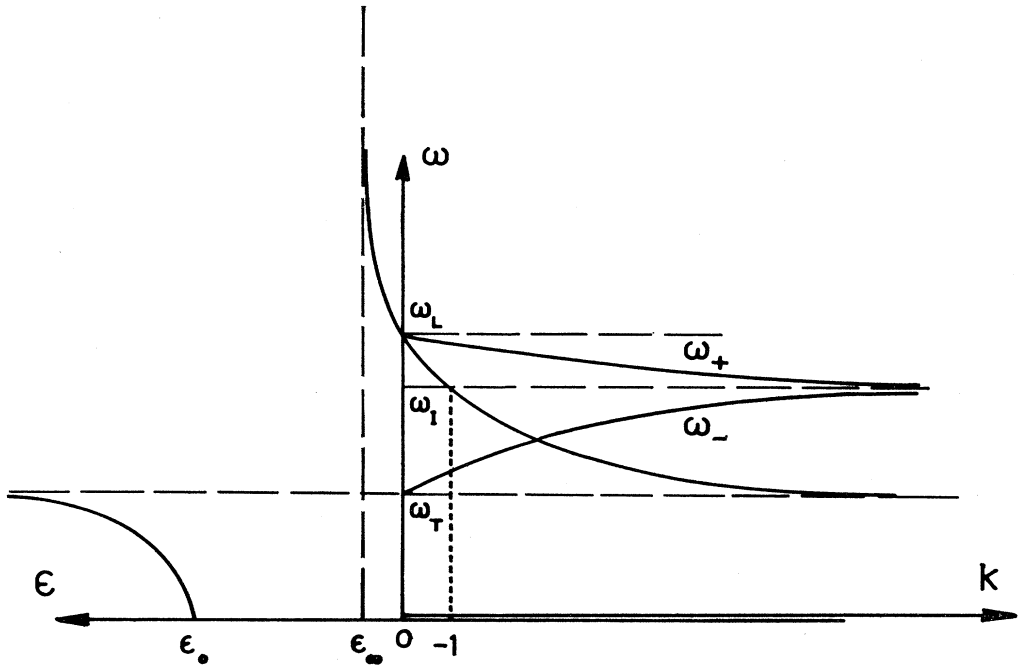

FIG. 4. On this drawing are plotted both the dispersion curves $\omega_+(k)$, $\omega_-(k)$ for the surface phonon modes of the slab and the dielectric constant as a function of frequency. One has $\epsilon(\omega_I)=-1$.

The integration is trivial for the bulk loss (26b) and gives

$$W_B^{\mathrm{NR}}(\omega)=-\frac{e^2L}{2\pi\hbar v^2}\ln\left(K^2\frac{v^2}{\omega^2}+1\right)\mathrm{Im}\frac{1}{\epsilon}. \quad (28)$$

This bulk loss spectrum has the Lorentzian shape

$$\mathrm{Im}\frac{1}{\epsilon}=\frac{\gamma}{\epsilon_\infty}\frac{x(1-x_L^2)}{(x_L^2-x^2)^2+\gamma^2x^2}, \quad \left(x=\frac{\omega}{\omega_T}\right) \quad (29)$$

strongly peaked at $\omega=\omega_L$ ($x=x_L$) and, of course, corresponds to the excitation of the longitudinal bulk phonon by the passing electron.

The nonretarded surface loss contribution

$$W_S^{\mathrm{NR}}(\omega)=2\pi\int_0^K kdk\, P_S^{\mathrm{NR}}(k,\omega) \quad (30)$$

has been estimated numerically in Ref. 2. If γ is small ($\gamma\simeq 10^{-2}$ for LiF) then (29) contributes but a δ function at $\omega=\omega_L$ and one can expect that (30) provides the main loss mechanism. Here we want to perform analytically the k integration involved in (30). This can be done, at least when ϵ is real, in the following way. If $\gamma=0$ then the expression in square brackets in (26a) is a real function of k. Therefore, the only contributions to (30) arise from the poles of P_S^{NR}, i.e., from the zeros of its denominator

$$D(k,\omega)=(1-\epsilon)^2e^{-kL}-(1+\epsilon)^2e^{kL}. \quad (31)$$

Writing

$$D(k,\omega)=D_+(k,\omega)D_-(k,\omega), \quad (32)$$

where

$$D_+=(1-\epsilon)e^{-kL/2}+(1+\epsilon)e^{kL/2}, \quad (33)$$

$$D_-=(1-\epsilon)e^{-kL/2}-(1+\epsilon)e^{kL/2}, \quad (34)$$

the equations $D_+=0$ and $D_-=0$ precisely define the dispersion curves $\omega_-(k)$ and $\omega_+(k)$ for the two (symmetrical and antisymmetrical) surface modes of the slab, respectively (Fig. 4). Explicitly, we have

$$D_-=0: \quad k_+=\frac{1}{L}\ln\left(\frac{1-\epsilon}{1+\epsilon}\right) \quad \text{for } \omega>\omega_I, \quad (35)$$

$$D_+=0: \quad k_-=\frac{1}{L}\ln\left(\frac{\epsilon-1}{1+\epsilon}\right) \quad \text{for } \omega<\omega_I, \quad (36)$$

where

$$\omega_I=\omega_T\left(\frac{\epsilon_0+1}{\epsilon_\infty+1}\right)^{1/2} \quad (37)$$

is the limiting frequency of the two surface modes (see Fig. 4). In order to obtain the contribution of those two simple poles [(35), (36)] we make use of the theorem

$$\lim_{\eta\to 0}\frac{1}{X-X_0\pm i\eta}=PP\frac{1}{X-X_0}\mp i\pi\delta(X-X_0) \quad (38)$$

or, rather, a straightforward generalization of it

$$\lim_{\eta\to 0}\frac{1}{f(x)\pm i\eta}=PP\frac{1}{f(x)}\mp i\pi\sum_i\frac{1}{|f'(x_i)|}\delta(x-x_i), \quad (39)$$

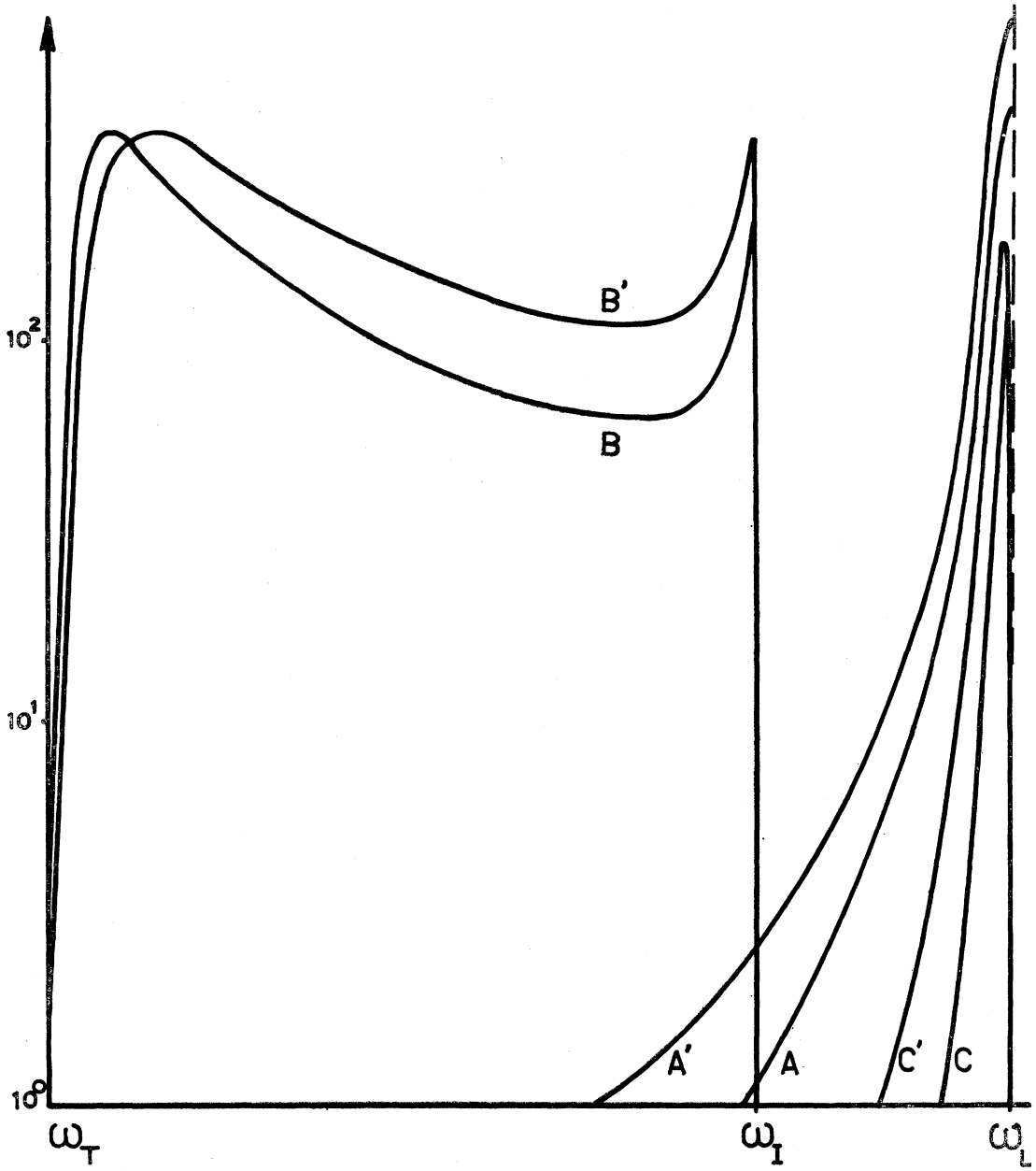

FIG. 5. Nonretarded loss spectrum for LiF on a semilogarithmic scale. The parameters appropriate to this crystal are $\epsilon_\infty=1.92$, $\epsilon_0=9.27$, $\omega_T=5.78\ 10^{13}\ \text{sec}^{-1}$, $\gamma=0.04$. The functions (28), (42), and (43) are plotted separately as curves A, B, C (A', B', C'). The total loss spectrum is the sum of the three curves A, B, C (thickness $L=400$ Å) or A', B', C' ($L=700$ Å). Surface losses would be only slightly perturbed by the introduction of a small damping γ in the dielectric constant. Units: $e^2/\pi\hbar v^2$.

where $f'(x_i)$ is the derivative of $f(x)$ at the simple pole $x=x_i$. Thus, we write $\epsilon(\omega)=\epsilon_R(\omega)+i\epsilon_I(\omega)$ and obtain

$$\lim_{\epsilon_I\to 0}\frac{1}{D(k)}=PP\frac{1}{D(k)}-\frac{2\pi i}{LD_-|D_-|}\delta(k-k_-)$$

if $\omega<\omega_I$ or $\epsilon<-1$, (40)

and

$$\lim_{\epsilon_I\to 0}\frac{1}{D(k)}=PP\frac{1}{D(k)}+\frac{2\pi i}{LD_+|D_+|}\delta(k-k_+)$$

if $\omega>\omega_I$ or $\epsilon>-1$. (41)

Introducing (40) and (41) into (30), and noting that for ϵ real the principal parts of the integrals have a

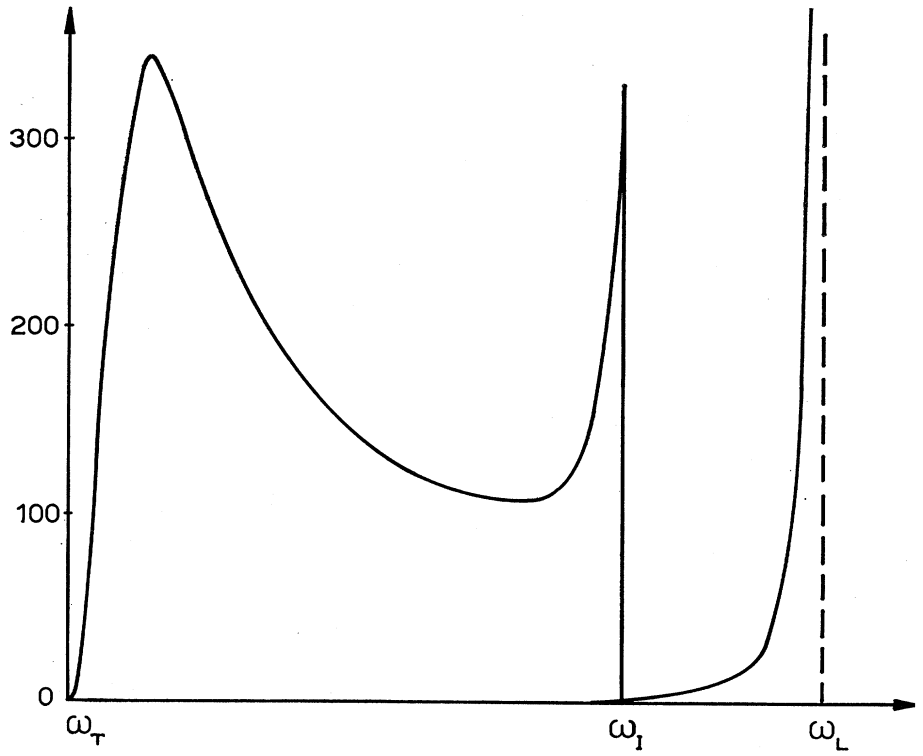

FIG. 6. Same as Fig. 5 on a linear scale. Thickness $L=700$ Å only is represented here. Surface and bulk spectra have been added in this figure (sum of curves A', B', C' in Fig. 5).

vanishing imaginary part, the integration is now trivial and we finally get

$$W_S^{\mathrm{NR}}(\omega)=-\frac{e^2}{\pi\hbar v^2}\frac{4\pi k_-^2L^{-1}}{(k_-^2+\omega^2/v^2)^2}\frac{\epsilon-1}{\epsilon(\epsilon+1)}\cos^2\frac{\omega L}{2v}\times\theta(K-k_-)\quad\text{if}\quad\omega_T<\omega<\omega_I \tag{42}$$

and

$$W_S^{\mathrm{NR}}(\omega)=-\frac{e^2}{\pi\hbar v^2}\frac{4\pi k_+^2L^{-1}}{(k_+^2+\omega^2/v^2)^2}\frac{1-\epsilon}{\epsilon(\epsilon+1)}\sin^2\frac{\omega L}{2v}\times\theta(K-k_+)\quad\text{if}\quad\omega_I<\omega<\omega_L, \tag{43}$$

where θ is the step function

$$\theta(x)=0\quad\text{for}\quad x<0$$
$$=1\quad\text{for}\quad x>0.$$

Formulas (42) and (43) essentially give the exact surface loss; the introduction of a small, frequency-independent damping constant γ in the dielectric constant would only slightly perturb this result. For example, it will somewhat smooth out the sharp discontinuity at $\omega=\omega_I$ and will provide some tailing for $\omega\lesssim\omega_T$ and $\omega\gtrsim\omega_L$. The tailing at $\omega\gtrsim\omega_L$ is of course negligeable compared to the resonant bulk loss (28) while the tailing at $\omega\lesssim\omega_T$ may be comparable to the Cherenkov loss which is studied in the next section.

In Fig. 5, the functions (28), (42), and (43) are plotted separately on a semilog diagram for LiF crystal slabs. Figure 6 gives the same on a linear scale. Figure 7 shows the shift of the surface loss peak when the slab thickness increases. This linear shift is easily understood when analyzing (42) and (36) as a function of L. Indeed, $W_S^{\mathrm{NR}}(\omega\to\omega_T)$ is proportional to

$$F(k)=\frac{k_-^2L^{-1}}{(k_-^2+a^2)^2}e^{k-L}\tanh\tfrac{1}{2}k_-L,\quad a=\frac{\omega}{v}. \tag{44}$$

In the region of interest, $k_-L\ll1$ and $e^{k-L}\sim1$, $\tanh\frac{1}{2}k_-L\sim\frac{1}{2}k_-L$. Therefore $F(k_-)$ is maximum where $k_-^3/(k_-^2+a^2)^2$ is maximum, i.e., when $k_-^2=3a^2$. Inverting (36), one finds for the frequency of the maximum surface loss

$$\omega_M\simeq\omega_T\left(\frac{1+\frac{1}{2}\sqrt{3}\,\epsilon_0(\omega_TL/v)}{1+\frac{1}{2}\sqrt{3}\,\epsilon_\infty(\omega_TL/v)}\right)^{1/2} \tag{45}$$

or

$$\omega_M\simeq\omega_T[1+\tfrac{1}{2}\sqrt{3}(\epsilon_0-\epsilon_\infty)\omega_TL/v)]. \tag{46}$$

This gives the differential shift

$$d\hbar\omega_M/dL=\tfrac{1}{2}\sqrt{3}(\epsilon_0-\epsilon_\infty)\hbar\omega_T(\omega_T/v)$$
$$\simeq1.5\times10^{-3}\ \mathrm{eV}/(100\ \text{Å}). \tag{47}$$

Figures 5–7 and Eqs. (46) and (47) are discussed in Sec. 4.

3. CHERENKOV LOSS

In this section, we study the exact form for the bulk loss, including retardation effects. One has, for the bulk

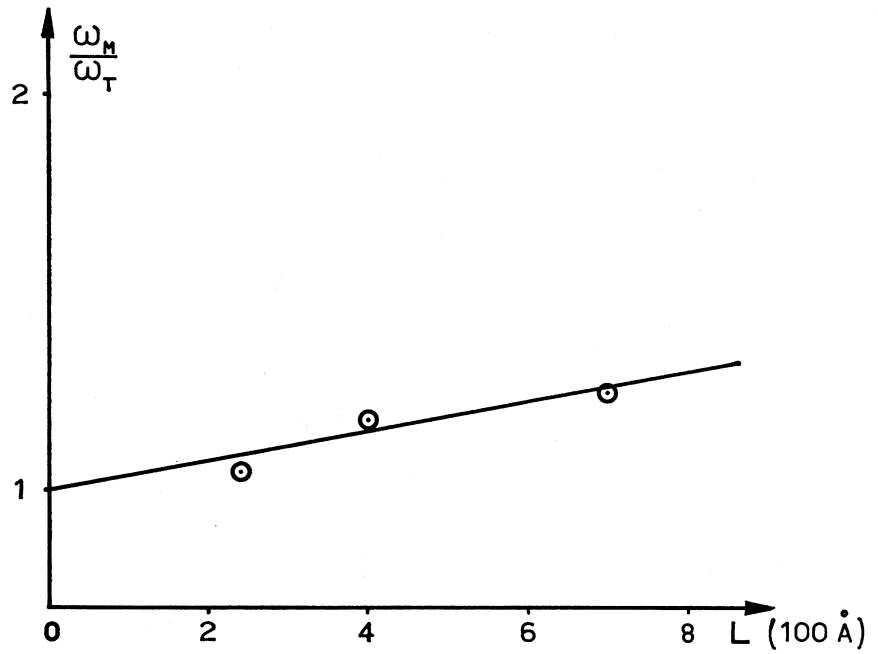

FIG. 7. Shift of the frequency at which the maximum surface loss occurs when the slab thickness is varied. The shift is nearly perfectly linear as explained in the text. Observed shift of the maximum loss frequency is given by the three experimental points indicated.

loss spectrum

$$W_B(\omega)=2\pi\int_0^K kdk\, P_B(k,\omega), \tag{48}$$

where P_B is given in (23):

$$W_B(\omega)=-\frac{e^2L}{\pi\hbar v^2}\operatorname{Im}\frac{\beta^2}{\epsilon}\int_0^K\frac{kdk}{\xi^2}. \tag{49}$$

From this formula, it is obvious that when $\epsilon(\omega)$ is real, the only contribution to the integral comes from the poles of the integrand, i.e., from the locus of points in the (ω,k) plane defined by

$$\xi^2=k^2-(\omega^2/v^2)(\epsilon(v^2/c^2)-1)=0. \tag{50}$$

This relation can be satisfied only if

$$\epsilon\frac{v^2}{c^2}-1>0. \tag{51}$$

Referring to Fig. 8, we see that this condition defines the so-called Cherenkov band[11] of frequencies $\omega_C<\omega<\omega_T$ within which the velocity of the passing electron is larger than the phase velocity associated with the lower polariton branch given by $\alpha=0$ or $\omega/k=c/\sqrt{\epsilon}$ [see Eq. (4)].

The threshold frequency ω_C is defined by (ϵ being real)

$$\epsilon(\omega_C)=c^2/v^2$$

or

$$\omega_C=\omega_T\left(\frac{c^2/v^2-\epsilon_0}{c^2/v^2-\epsilon_\infty}\right)^{1/2}. \tag{52}$$

[11] J. D. Jackson, *Classical Electrodynamics* (Wiley, New York, 1962), p. 499.

Relation (50) defines a curve denoted by Γ in Fig. 8. The part of this curve within region R_1, to the left of the line $\omega=kc$, corresponds to Cherenkov radiation flowing out of the slab [$\alpha_0=i\delta_0$, see Fig. 3(b)]. The part of Γ in region L_1, to the right of $\omega=kc$, represents Cherenkov light trapped into the slab as a result of total internal reflection at the slab boundaries. Indeed, from Eq. (50) one checks that Γ crosses the line $\omega=kc$ at a point such that $\epsilon=1+c^2/v^2$. Therefore, the angle θ of the Cherenkov cone defined by $\cos\theta=c/\sqrt{(\epsilon)}v$ is just the critical angle for total reflection satisfying $\sin\theta=1/\sqrt{\epsilon}$ (see Fig. 9).

Now we proceed to evaluate (49). Again, using (39), we write

$$\lim_{\epsilon I\to 0}\frac{1}{\xi^2}=PP\left(\frac{1}{\xi^2}\right)+\frac{i\pi}{2k}\delta(k-k_\omega), \tag{53}$$

where

$$k_\omega{}^2=(\omega^2/v^2)(\epsilon(v^2/c^2)-1). \tag{54}$$

One finds, when ϵ is real,

$$W_B(\omega)=0 \quad \text{if} \quad \omega<\omega_C, \tag{55a}$$

$$W_B(\omega)=-\frac{e^2}{\pi\hbar v^2}\frac{L\pi}{2}\frac{\epsilon(v^2/c^2)-1}{\epsilon}\times\left[\theta(\omega)-\theta\left(\omega-\frac{Kv}{\epsilon(v^2/c^2)-1}\right)\right] \tag{55b}$$

if

$$\omega_C<\omega<\frac{Kv}{\epsilon(v^2/c^2)-1}\simeq\omega_T,$$

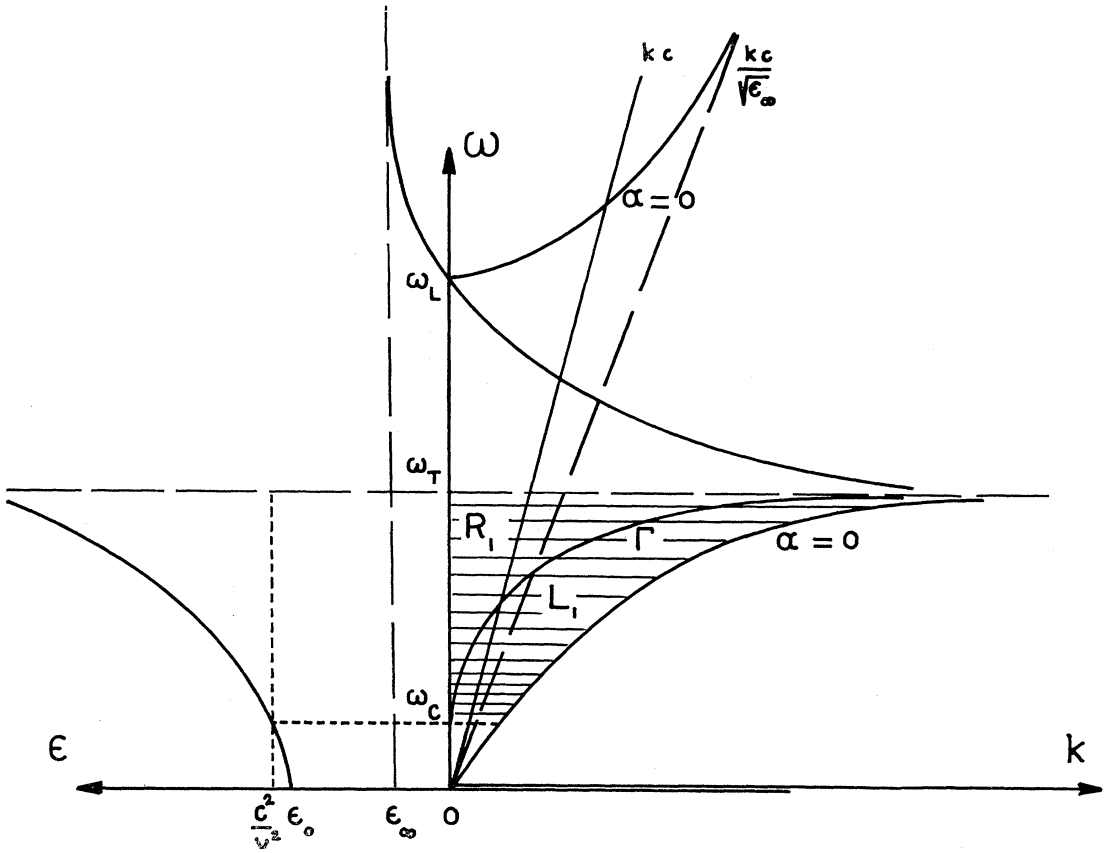

FIG. 8. Region of the (ω,k) plane where the Cherenkov condition (51) is satisfied (shaded area). Curve Γ, given by Eq (50), provides the dispersion relation for the emitted Cherenkov radiation. In region R_1, the radiation flows out of the slab whereas in region L_1, the Cherenkov cone undergoes total internal reflection at the slab surfaces.

and

$$W_B(\omega)=-\frac{e^2}{\pi\hbar v^2}\frac{L\pi}{4}\ln\left\{\frac{K^2(v^2/\omega^2)}{1-\epsilon(v^2/c^2)}+1\right\}$$

$$\times\frac{\epsilon_0-\epsilon_\infty}{\epsilon_0\epsilon_\infty}\delta(1-\omega/\omega_L)\quad\text{if}\quad\omega>\omega_T. \tag{55c}$$

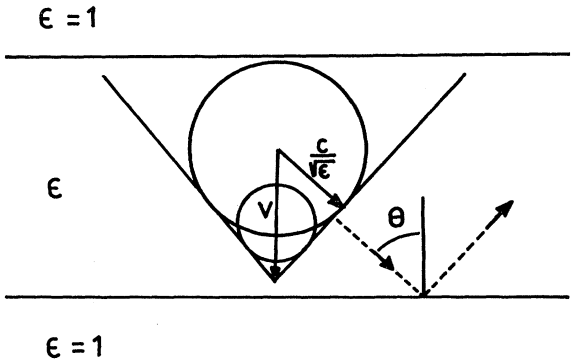

FIG. 9. Total internal reflection of the Cherenkov light cone at the slab boundaries. The angle θ of the cone defined by $\cos\theta=(c/v)\epsilon^{-1/2}$ is just the critical angle for total reflection when $\epsilon=1+c^2/v^2$.

When ϵ has an imaginary part, then the expression

$$W_B(\omega)=-\frac{e^2}{\pi\hbar v^2}L\,\mathrm{Im}\left[\frac{\beta^2}{\epsilon}\frac{1}{2}\ln\left\{\frac{K^2(v^2/\omega^2)}{1-\epsilon(v^2/c^2)}+1\right\}\right] \tag{56}$$

is valid everywhere: $0<\omega<\infty$. Results (55) and (56) are shown in Fig. 10 as curves A and B, respectively. The broken curve C in this figure represents the nonretarded bulk loss spectrum (28).

It is seen that the part of the energy lost in the bulk of the slab through the Cherenkov mechanism is peaked for $\omega\lesssim\omega_T$ where it dominates the loss to longitudinal phonon excitation. However, the height of the peak is three orders of magnitude smaller than the longitudinal peak so that the Cherenkov loss can only modify the low-energy tail of the nonretarded bulk loss spectrum.

We want to close this section by establishing the connection between our loss spectrum (55) and (56) and the results for the total bulk loss obtained long ago by Fermi.[7] According to (20), the total bulk loss is given by

$$W_B{}^{\mathrm{tot}}=\int_{-\infty}^{+\infty}d\omega\;\hbar\omega W_B(\omega) \tag{57}$$

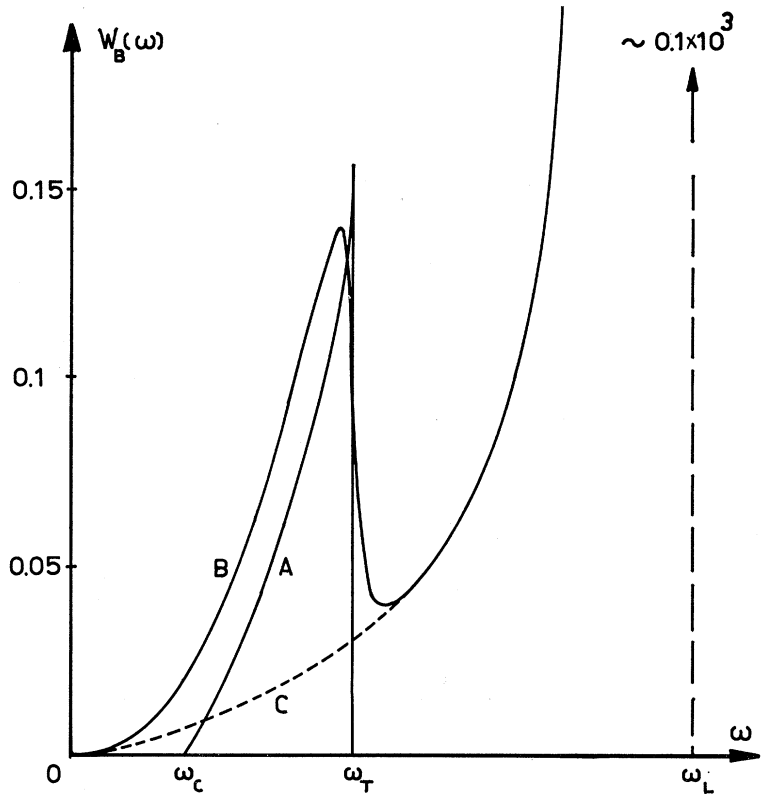

FIG. 10. Bulk energy-loss spectrum (in units $Le^2/\pi\hbar v^2$). Curve A: ϵ real; curve B: ϵ complex with $\gamma=0.04$; broken curve C: nonretarded loss spectrum.

and can be separated into two parts:

$$W_B{}^{\rm tot}=2\int_{\omega_C}^{\omega_T} W_B(\omega)\hbar\omega d\omega+2\int_{\omega_C}^{\infty} W_B(\omega)\hbar\omega d\omega$$
$$=W_{\rm CR}{}^B+W_{\rm LO}{}^B \qquad (58)$$

corresponding to losses through the Cherenkov radiation and through the coupling to the LO phonon, respectively.

Let us introduce (55) into (58). Two cases have to be distinguished[12]:

Case 1: $\epsilon_\infty<c^2/v^2<\epsilon_0$. Here the lower limit ω_C of the Cherenkov band is $\omega_C=0$ and we have

$$W_{\rm CR}{}^B=\frac{e^2}{v^2}\int_0^{\omega_T}\omega\frac{\epsilon(v^2/c^2)-1}{\epsilon}d\omega. \qquad (59)$$

The integration is elementary and gives

$$W_{\rm CR}{}^B=-\frac{e^2\omega_T{}^2}{2v^2}\left\{-\frac{v^2}{c^2}+\frac{1}{\epsilon_\infty}[1-(1-\epsilon_0/\epsilon_\infty)\times\ln(1-\epsilon_\infty/\epsilon_0)]\right\}. \qquad (60)$$

[12] If $\epsilon_\infty>c^2/v^2$, then the Cherenkov band extends at least to the next resonance of the dielectric constant, for example up to some characteristic electronic transition frequency in the visible or ultraviolet. Generalization of the theory to this situation or to the case where $\epsilon(\omega)$ has several resonances in a given frequency range, is straightforward.

Case 2: $c^2/v^2>\epsilon_0$. Then $\omega_C>0$ is given in (52). One finds

$$W_{\rm CR}{}^B=-\frac{e^2\omega_T{}^2}{2v^2}\left(1-\frac{\epsilon_0}{\epsilon_\infty}\right)\times\left[\frac{1-\epsilon_\infty(v^2/c^2)}{\epsilon_\infty-(c^2/v^2)}-\ln\left(1-\epsilon_\infty\frac{v^2}{c^2}\right)\right]. \qquad (61)$$

In both cases, integration of (55c) is trivial and gives

$$W_{\rm LO}{}^B=-\frac{e^2\omega_T{}^2}{2v^2}\frac{\epsilon_0-\epsilon_\infty}{\epsilon_\infty{}^2}\ln\left(\frac{K^2v^2}{\omega_L{}^2}+1\right). \qquad (62)$$

One sees that contributions (60) or (61) are independent of the cutoff momentum transfer K. They represent true radiation transporting the energy lost by the beam at an arbitrary, large distance K^{-1} from the electron path (here ϵ is real). The longitudinal loss (62) on the contrary goes to zero with K which means that the excitation energy of the LO phonon remains localized around the beam axis.

Results (60)–(62) are in complete agreement with expressions (37), (36), and (30) in Fermi's paper[7] provided one makes the replacements

$$\epsilon_\infty\to 1,\quad \omega_T{}^2\to\omega_p{}^2/(\epsilon_0-1)$$

and

$$K^2\to\frac{3.17}{4}\frac{\epsilon_0}{\epsilon_0-1}\frac{1}{b^2}.$$

This somewhat arbitrary relationship between our limiting wave vector K and Fermi's cylinder radius b is due to the arbitrariness involved in both cases when unrelated sharp cutoffs are introduced either in K space or in real R space.

4. DISCUSSION AND CONCLUSIONS

The classical processes by which a fast-charged particle loses some of its energy in passing through a polar dielectric slab can be divided into bulk loss processes, proportional to the path length, and surface losses, essentially independent of the slab thickness. In turn, each of these classes contains nonradiative and radiative mechanisms: the LO resonant loss and the Cherenkov radiation on the one hand, the localized polariton excitation and the radiative or virtual-mode excitation (yielding "transition radiation") on the other hand.

In this paper the bulk losses have been thoroughly investigated while the surface losses have been treated in the quasistatic approximation. The main results concerning LiF can be listed as follows:

(a) For slab thicknesses up to a few thousand angstroms, the surface-loss spectrum, extending from ω_T to ω_L, dominates the bulk losses (see Figs. 5 and 6). The shape of the spectrum, in particular the existence of a peak close to ω_I and of a dip between ω_I and ω_L, agrees with the numerically computed spectrum of Ref. 2. However, we do not find, in the integrated surface loss, any contribution which would reduce the LO peak at ω_L [as suggested by the analysis of Ref. 2, Eq. (4.2)]. Rather, the LO peak is enhanced by a maximum in the surface loss occurring very close to ω_L (Fig. 5).

(b) The maximum of the surface loss is nearly independent of the slab thickness L whereas its position shifts linearly with L.[13] These features are also exhibited by the experimental loss peak[1] (see Fig. 7).

(c) A meaningful comparison between our theoretical curve of Fig. 6 and the experimental one in Fig. 1 could be made in the following way. With the loss functions $W_B{}^{\mathrm{NR}}(\omega)$ and $W_S{}^{\mathrm{NR}}(\omega)$ [Eqs. (28), (42), and (43)] which are plotted in Fig. 6, one can define an observable loss spectrum by

$$W(\omega)=\frac{1}{2\Delta}\int_{\omega-\Delta}^{\omega+\Delta}[W_B{}^{\mathrm{NR}}(\omega')+W_S{}^{\mathrm{NR}}(\omega')]d\omega', \quad (63)$$

where $\pm\Delta\hbar$ represents the accuracy with which the detector can measure energy losses. In the experiments of Boersch *et al.*,[1] one has $\Delta\hbar\simeq 0.01$ eV. The integration in (63) will smooth out any sharp feature of the loss functions. Thus the sharp peak at ω_I in $W_S{}^{\mathrm{NR}}$ will be replaced by a shoulder of the kind observed in the experimental spectrum around 0.08 eV. Also the strong, narrow bulk loss peak at ω_L will be averaged out and will give a broad peak in $W(\omega)$ similar to but somewhat bigger than the observed bump in the high-energy tail of the experimental curve around 0.1 eV.

In part II of this work, we will present a detailed comparison of this kind but using the full retarded loss spectrum.

(d) The Cherenkov bulk loss contributes a low-energy tailing ($\omega<\omega_T$) to the spectrum. Referring to Eq. (24), one sees that a similar effect should result in the radiative surface loss (denominators ξ^2) in addition to the transition-radiation effect (resonant denominator Δ). However, one cannot assert the relative efficiency of these various mechanisms before one has explicitly computed (24).

The identity of our results (55) and (56) concerning the total bulk loss with those of Fermi[7] illustrates the equivalence of the two definitions of the energy loss: either as the work done by the fields on the charged particle or as the flux of the Poynting vector through a closed surface around the particle trajectory. Of course, if one is interested in obtaining the photon emission alone, the second method seems more natural.

(e) We have not been able so far to obtain an analytical result for the radiative surface losses. Only the contribution from the excitation of real, surface polariton modes (α_0 and α real) can be obtained exactly if ϵ is real and this provides a useful check for computer calculations on the transition radiation. This will be treated in a subsequent paper.

(f) An interesting situation arises when, like in the displacive class of ferroelectrics, a transverse optical mode frequency is strongly temperature dependent. If surface-phonon excitations do provide the main source of energy loss, one should be able to observe according to (46) a Curie-type behavior of the maximum loss frequency in thin ferroelectric slabs like $BaTiO_3$. Also in these materials of very high dielectric constants, the Cherenkov zone extends far in the high-frequency region even for relatively low electron velocities, so that the Cherenkov loss will give a significant contribution over a wide energy range.

[13] In Ref. 2 the maximum computed surface loss seems to depend on the slab thickness and its frequency shift is not clearly defined.